Simultaneous characterization of temperature   and ve lo ci ty profiles using time reversal:

Numerical study of free convection

Simultaneous characterization of temperature and velocity profiles using time reversal: Numerical study of free convection

A. Maurel[1] and G. Bouchet[2]

[1] *Laboratoire Ondes et Acoustique, UMR CNRS 7587, Ecole Supérieure de Physique et de Chimie Industrielles - 10 rue Vauquelin, 75005 Paris, France*
[2] *Institut de Mécanique des Fluides, UMR CNRS 7507*
2 rue Boussingault, 67000 Strasbourg, France

Abstract. – We present an acoustical method, based on time reversal, for simultaneous characterization of temperature and velocity profiles. The method is numerically validated in a case of free convection; the acoustic propagation is obtained from calculations of ray propagation and the convective flow is described by analytical profiles or by fields stemmed from numerical simulation. The ray theory approximation, used to solve the inverse problem, is discussed.

Introduction. – Most of the usual techniques for temperature measurement are local and intrusive (hot-wire probe, hot-film sensors, thermocouples). Some optical techniques such as low-contrast shadowgraphy, visualization with thermal camera or induced fluorescence measurement are examples of non-intrusive methods but can be used only for translucid fluids. Furthermore, simultaneous measurement of the velocity field is not possible, or requires the use of another technique. Among these techniques, acoustic waves provide a direct, non-intrusive and non-localized way of probing hydrodynamic flow fields. Several approaches have been proposed in the literature, *e.g.* ultrasound scattering [1, 2] or tomography [3]. When the acoustic wavelength is small compared with the characteristic length of the flow and for small Mach numbers, the description of the sound flow interaction is restricted to geometrical acoustics; in this context, an ultrasonic technique, based on the time reversal process, has been developed recently to study the structure and dynamics of localized vortices [4, 5]; the presented work extends this method by including a simultaneous measurement of a temperature profile. The aim of this paper is to develop and to numerically validate the method, that can be used as an investigation tool on an experimental set-up.

Principle. – In the limit where the frequency of the sound wave is very large compared to the typical frequencies of the problem, a Hamiltonian system can be derived from the wave equation for sound ray propagation [6]:

$$\begin{cases} \dfrac{\mathrm{d}\boldsymbol{r}}{\mathrm{d}t} = \dfrac{\partial \omega}{\partial \boldsymbol{k}}, \\ \dfrac{\mathrm{d}\boldsymbol{k}}{\mathrm{d}t} = -\dfrac{\partial \omega}{\partial \boldsymbol{r}}, \end{cases} \tag{1}$$
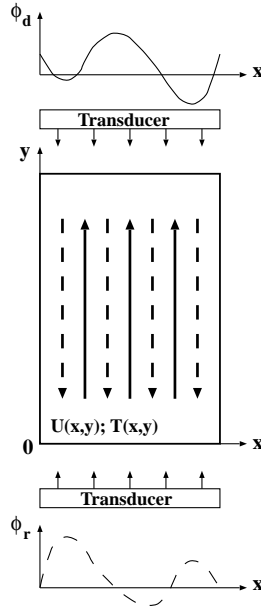
Fig. 1 – Configuration of the study.

where $\omega(\boldsymbol{r}, \boldsymbol{k})$ is the wave pulsation, $\boldsymbol{r}$ the sound ray position and $\boldsymbol{k}$ the wave vector. In a fluid at rest with uniform temperature T_0, the usual relation $\omega_0 = c_0 k$ describes a straight ray propagation. With a fluid flowing with velocity $\boldsymbol{u}(\boldsymbol{r})$ in a non-uniform temperature field with a thermal fluctuation of magnitude T, the pulsation writes $\omega(\boldsymbol{r}, \boldsymbol{k}) = c(T)k + \boldsymbol{u}(\boldsymbol{r}) \cdot \boldsymbol{k}$; $c(T)$ is the sound speed with temperature dependence, written at first order in T: $c(T) = c_0(1 + \alpha T)$, where α is the thermal expansion coefficient. System (1) becomes

$$\begin{cases} \dfrac{\mathrm{d}\boldsymbol{r}}{\mathrm{d}t} = c_0(1 + \alpha T)\dfrac{\boldsymbol{k}}{k} + \boldsymbol{u}\,, \\ \dfrac{\mathrm{d}\boldsymbol{k}}{\mathrm{d}t} = -c_0 \alpha k \boldsymbol{\nabla} T - (\boldsymbol{k} \cdot \boldsymbol{\nabla})\boldsymbol{u} - \boldsymbol{k} \wedge (\boldsymbol{\nabla} \wedge \boldsymbol{u})\,. \end{cases} \tag{2}$$

This system can be integrated to determine the ray trajectories (see section *Numerical experiment*). However, it is useful to simplify system (2) for small values of u/c_0 and αT; in this latter case, two main effects of the flow on the sound ray can be isolated, with $\boldsymbol{v} = \partial_t \boldsymbol{r} = v\boldsymbol{n}$:

1) the fluid motion and temperature inhomogeneity result in a local modification of the sound speed:

$$v = c_0(1 + \alpha T) + \frac{\boldsymbol{u} \cdot \boldsymbol{k}}{k}\,; \tag{3}$$

2) the flow vorticity and the thermal gradients locally modify the direction of the wave propagation:

$$\frac{\mathrm{d}\boldsymbol{n}}{\mathrm{d}t} = -c_0 \alpha \boldsymbol{\nabla} T + (\boldsymbol{\nabla} \wedge \boldsymbol{u}) \wedge \boldsymbol{n}\,. \tag{4}$$

In an experiment of time reversal, we use two transducer arrays placed in front of each other on both sides of the flow as shown in fig. 1. The first array sends a plane wave in the y-direction across the flow (direct way). The second array records the signal $\phi_{\mathrm{d}}(x)$, corresponding to the direct time of flight $t_{\mathrm{d}}(x)$. Then time reversing the wave consists for each transducer of the

second array in re-emitting the recorded signal after the sign of time has been changed, or in other words, in emitting first the last part of the received signal. Finally, the first array receives the "time-reversed" signal $\phi_r(x)$, corresponding to the time denoted $t_r(x)$. A "blank" time of flight is defined in the fluid at rest at uniform temperature, leading to $t_d^0(x)$ and $t_r^0(x)$. The time reversal procedure is known to compensate scalar inhomogeneities of the medium: in the experiment described above, the wave, distorted after crossing a scalar-inhomogeneous medium and time-reversed, recovers its initial shape after re-propagation through the medium. On the other hand, it is expected and has been experimentally improved that a vectorial inhomogeneity, such as the velocity flow field, violates the time reversal invariance [7]. In this latter case, the effect of the vectorial inhomogeneity on the wave is amplified by the time reversal procedure. In the present case with both scalar (temperature fluctuation) and vectorial (velocity flow field) inhomogeneities, it is expected that the direct time of flight contains both signatures of T and $\boldsymbol{u}$ while the time-reversed signal only contains the signature of $\boldsymbol{u}$.

To solve the inverse problem $(t_d, t_r) \rightarrow (\boldsymbol{u}, T)$, we use eq. (3) in the approximation of geometrical acoustics. The time shifts are defined as $\Delta t_d = t_d(x) - t_d^0(x)$ and $\Delta t_r = t_r(x) - t_r^0(x)$. Using (3) in the hypothesis of straight line propagation ((4) is not taken into account; this is discussed in the section *Discussion*) leads to system (5):

$$\begin{cases} \Delta t_d = t_d(x) - t_d^0(x) \sim -\dfrac{H}{c_0}\left(\dfrac{\langle u_y \rangle}{c_0} + \alpha \langle T \rangle\right), \\ \Delta t_r = t_r(x) - t_r^0(x) \sim \dfrac{2H}{c_0^2}\langle u_y \rangle. \end{cases} \qquad (5)$$

In this system, it appears that only a mean value of the temperature and velocity field is obtained, the average occurring along the ray propagation in the y-direction. As expected, $\Delta t_r(x)$ does not depend anymore on the temperature field since, in system (2), the velocity field $\boldsymbol{u}$ breaks the time reversal symmetry, *i.e.* $\mathcal{T}$: $t \rightarrow -t$ and $\boldsymbol{k} \rightarrow -\boldsymbol{k}$, while the temperature leaves (2) invariant by this transformation. Finally, the mean velocity and temperature profiles can be written:

$$\begin{cases} \langle u_y \rangle(x) = -\dfrac{c_0^2}{2H}\Delta t_r(x), \\ \langle T \rangle(x) = \dfrac{c_0}{\alpha H}\left(\dfrac{\Delta t_r(x)}{2} - \Delta t_d(x)\right). \end{cases} \qquad (6)$$

Numerical experiment. – We consider a flow induced by buoyancy effect between two vertical walls of length H (y-direction) differentially heated (ΔT between the two walls at $x = 0$ and $x = L$). In this configuration, a horizontal temperature gradient appears in the x-direction between the walls. This temperature gradient is responsible for the development of a convection roll. The thermo-gravity force $\rho \alpha \Delta T g$ (ρ is the density and g the gravity) induces fluid motion to the top along the hot wall and to the bottom along the cold one. With ν the kinematic viscosity and κ the thermal diffusivity, it is possible to specify the flow by three dimensionless parameters: the Rayleigh number $Ra = \alpha g \Delta T L^3/(\kappa \nu)$, the Prandtl number $Pr = \sqrt{\nu/\kappa}$ and the aspect ratio $a = L/H$. At low Rayleigh number, the temperature gradient is constant and the roll invades the whole cell; this regime corresponds to the basic flow, independent of the y-direction [8]. With increasing further Ra, a secondary regime appears, associated with the development of a vertical temperature gradient [9]; horizontal velocity and temperature gradients concentrate in the boundary layers near the walls (S-shaped profiles). Finally, at high Rayleigh numbers, the flow becomes turbulent. The whole dynamics occurs in the turbulent boundary layers and the center of the cells is a slack region. In the following, we consider a configuration where the aspect ration of the cell a is small so that the flow is mainly vertical with a weak dependence on the y-direction.

The field variables can be conveniently dimensionless by choosing units of length, temperature and velocity: H, ΔT and c_0. We take $U = \sqrt{\kappa\nu}/L$ for the characteristic velocity of the flow (used in $Ma = U/c_0$). The dimensionless temperature is written as θ and $\tilde{X}$ refers to the dimensionless form of X. System (2) takes the form

$$\frac{\mathrm{d}\tilde{\boldsymbol{r}}}{\mathrm{d}\tilde{t}} = (1 + Ma_T\theta)\frac{\boldsymbol{k}}{k} + Ma\tilde{\boldsymbol{u}}\,, \tag{7}$$

$$\frac{\mathrm{d}\boldsymbol{k}}{\mathrm{d}\tilde{t}} = -Ma_T k\boldsymbol{\nabla}\boldsymbol{\theta} - Ma((\boldsymbol{k}\cdot\boldsymbol{\nabla})\tilde{\boldsymbol{u}} - \boldsymbol{k}\wedge(\boldsymbol{\nabla}\wedge\tilde{\boldsymbol{u}})\,. \tag{8}$$

In the numerical experiment, the following procedure is chosen: the system is numerically integrated using a fourth-order Runge-Kutta scheme with adaptive step size. The initial conditions are at $\tilde{t} = 0 : \tilde{\boldsymbol{r}} = (\tilde{x}(i), 0)$ with $\tilde{x}(i) = ia/N$ and $\boldsymbol{k} = (0, 1)$. The N ray trajectories are integrated until $\tilde{y} = 1$ and we denote $\tilde{x}_f(i)$ and $\boldsymbol{k}_f(i)$ the position and the wave vector at $\tilde{y} = 1$. The direct time of flight between $\tilde{y} = 0$ and 1 is denoted $\tilde{t}_\mathrm{d}(i)$; the blank time of flight is equal to 1. The back way is integrated using the following initial conditions at $\tilde{t}(i) = \tilde{t}_\mathrm{a} - \tilde{t}_f(i)$, where $\tilde{t}_\mathrm{a}$ is an arbitrary constant such that $\tilde{t}(i) > 0$: $\tilde{\boldsymbol{r}} = (\tilde{x}_f(i), 1)$ and $\boldsymbol{k} = -\boldsymbol{k}_f(i)$. These conditions correspond to the transformation $\mathcal{T}$ of time reversal. Here, $\tilde{t}_\mathrm{b}^0 = \tilde{t}_\mathrm{a}$.

Analytical profiles for the basic and secondary flow. For low Rayleigh numbers, the flow is invariant of the $\tilde{y}$ variable and can be described in a dimensionless form by

$$\begin{cases} \theta(\tilde{x}) = \tilde{x}/a\,, \\ \tilde{u}_y(\tilde{x}) = -\dfrac{Ra}{6a^3 Pr}\tilde{x}(\tilde{x} - a/2)(\tilde{x} - a)\,. \end{cases} \tag{9}$$

To take into account the finite dimension of the cavity and to obtain a solution for higher Rayleigh numbers, a dependence on the y-direction has to be considered. Elder [9] shows
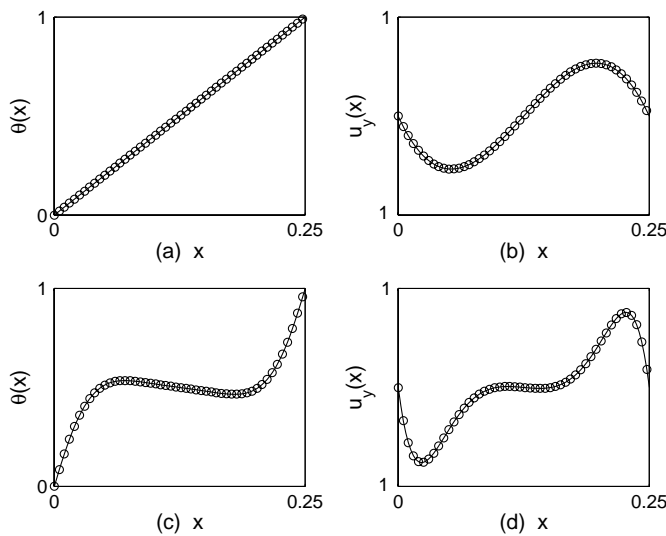
Fig. 2 – Analytical (–) and reconstructed (○) profiles for the basic ((a) temperature and (b) velocity) at $Pr = 15$, $Ra = 10^3$, $Ma = 10^{-7}$, $Ma_T = 10^{-6}$ and for the secondary flow ((c) temperature and (d) velocity) at $Pr = 15$, $Ra = 10^4$, $Ma = 10^{-6}$, $Ma_T = 10^{-5}$.
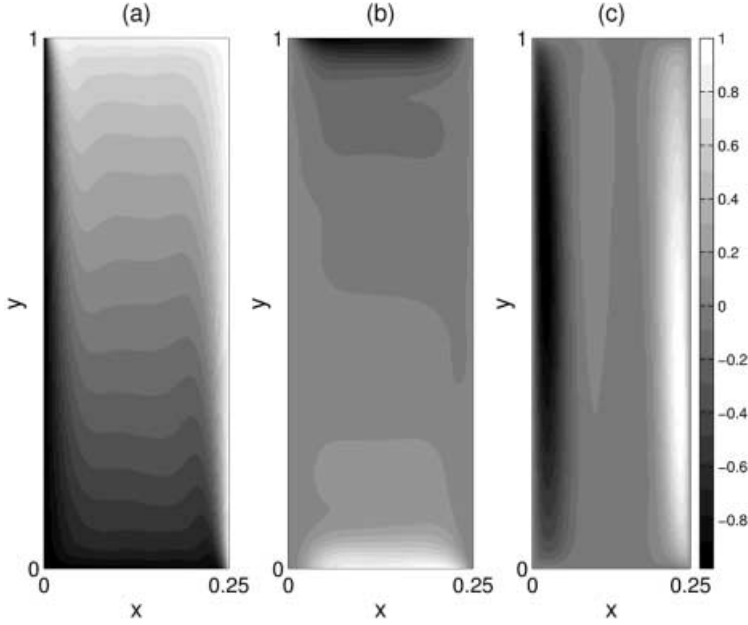
Fig. 3 – Temperature (a) and velocity ((b) $\tilde{u}_x$, (c) $\tilde{u}_y$) fields from numerical simulation of Navier-Stokes equations ($Pr = 15$, $Ra = 10^4$, $Ma = 10^{-6}$, $Ma_T = 10^{-5}$).

that a secondary flow occurs in laminar regime for moderated Rayleigh numbers where the temperature field depends on the y-direction through the constant coefficient $\beta = \mathrm{d}\theta/\mathrm{d}\tilde{y}$. The temperature and velocity fields are given by

$$\begin{cases} \theta(\tilde{x}) = \theta_m(\tilde{y}) + f\left[e^{-m\tilde{x}}\cos m\tilde{x} - e^{m(\tilde{x}-a)}\cos m(\tilde{x}-a)\right], \\ \tilde{u}_y(\tilde{x}) = \dfrac{2m^2}{\beta Pr}f\left[e^{-m\tilde{x}}\sin m\tilde{x} + e^{m(\tilde{x}-a)}\sin m(\tilde{x}-a)\right], \end{cases} \tag{10}$$

where $\theta_m(\tilde{y}) = 0.5 + \beta(\tilde{y} - 0.5)$. f is a numerical constant of order 0.5 and $ma = (\beta Ra/4)^{1/4}$.

Figure 2 shows the analytical and reconstructed profiles for $Pr = 15$, in an experiment performed for the basic flow at $Ra = 10^3$, $Ma = 10^{-7}$ and $Ma_T = 10^{-6}$ and for the secondary flow at $Ra = 10^4$, $Ma = 10^{-6}$ and $Ma_T = 10^{-5}$; the aspect ratio of the cell corresponds to $a = 1/4$. A good agreement between the analytical and reconstructed profiles is obtained. This agreement is mainly due to the fact that the temperature and velocity profiles do not contain strong gradients. This ensures the validity of the straight line propagation hypothesis and consequently, the validity of the reconstruction technique.

Real profiles obtained from numerical simulation of Navier-Stokes equations. The analytical profiles used above do not include the horizontal velocity component that contributes to the recirculation motion near the two horizontal walls at $\tilde{y} = 0$ and 1. In order to have a real field, we have performed numerical simulations of the Navier-Stokes equations using a code based on the finite spectral element method. The temperature and velocity fields obtained for $Pr = 15$, $Ra = 10^4$, $Ma = 10^{-6}$ and $Ma_T = 10^{-5}$ are shown in fig. 3; fig. 4 compares the reconstructed profiles with the mean profiles obtained from the numerical simulation. Again, a good determination of the real mean profiles is obtained, even if, in this latter case, local temperature and velocity gradients produce refraction effects. This
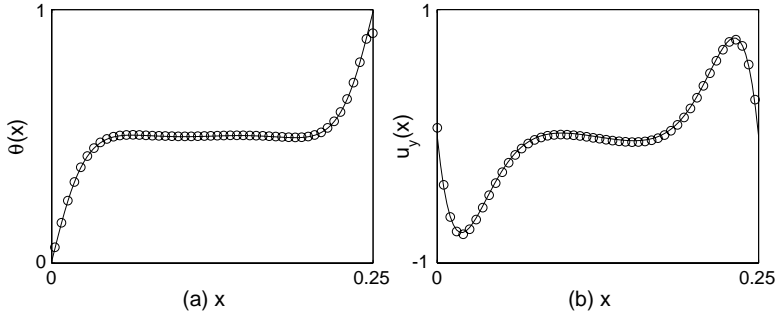
Fig. 4 – Real mean profile from numerical simulation (−) and reconstructed profile (∘) for (a) the temperature and (b) the $\tilde{u}_y$ velocity.

refraction is visible on the reconstructed profiles; if the initial shift in $\tilde{x}$ is constant and equal to a/N, the position $\tilde{x}_f$ is no regular anymore: rays are concentrated in the profile center. However, this does not affect significantly the shape of the reconstructed profiles, because the refraction effects remain small at these Ma and Ma_T values (see section *Discussion*).

Discussion. – The presented results have been obtained using a reconstruction technique based on geometrical acoustics. This approximation is particularly well adapted to such a technique. Indeed, it is valid as long as the sound frequency f is large compared with the typical frequencies of the problem. This implies $f \gg c/\delta, U/\delta$ and U/λ, where λ is the sound wavelength and where $\delta \sim T/\nabla T, U/\nabla U$ is the typical length of the velocity or temperature gradients. Since the condition $Ma \ll 1$ is always satisfied in the considered subsonic flows, the main limitation occurs when very strong gradients produce very small δ values, such as
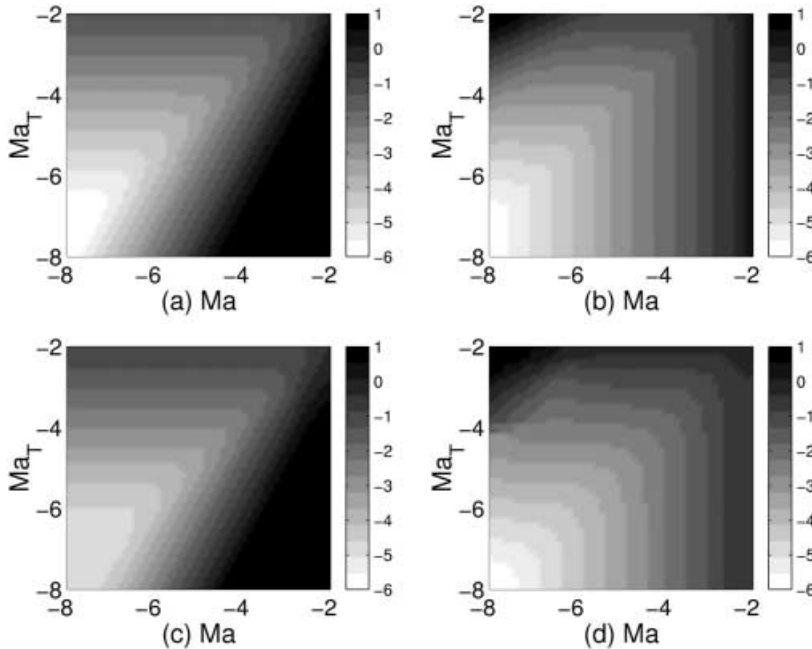
Fig. 5 – Diagram of the error between real and reconstructed profile varying Ma and Ma_T, for the basic flow ((a) on θ and (b) on $\tilde{u}_y$) and for the secondary flow ((c) on θ and (d) on $\tilde{u}_y$).

localized structures produced by strong gradients in a turbulent flow [10].

On the other hand, the presented technique is possible when the mean velocity profile is meaningful; of course, if the flow fields need to be determined in the details of y-direction, tomography methods are to be considered.

Even when the mean profiles are meaningful, the main limitation of the method comes from the hypothesis —used in the reconstruction— of straight line propagation; in order to quantitatively estimate this limitation, we have calculated the errors, corresponding to the mean difference between the reconstructed and real profiles when these latter are analytically known (basic and secondary flows). Figure 5 shows the results in both cases for the temperature and velocity reconstructions. The error has two origins, both related to the spatial shift $\Delta \tilde{x}$ between the two arrays. Because of the deflection, the real distance covered by the ray is not equal to 1, as used in the reconstruction, but equal to $\sqrt{1 + \Delta \tilde{x}^2} \sim 1 + \Delta \tilde{x}^2/2$. However, it can be easily shown from (4) that $\Delta \tilde{x} \sim \theta \sim \int_S ||\boldsymbol{n} \wedge \partial_{\tilde{t}} \boldsymbol{n}||$ is of order 1 in Ma, Ma_T; the corresponding error δt on the time of flights is of order 2: $\delta t \sim Ma^2$, Ma_T^2. This justifies *a posteriori* that the reconstruction neglects the ray deflection. Another consequence of the spatial shift comes from an erroneous position for $\theta(\tilde{x})$ instead of $\theta(\tilde{x} + \Delta \tilde{x})$ (or $\tilde{u}(\tilde{x})$ instead of $\tilde{u}(\tilde{x} + \Delta \tilde{x})$). From fig. 5, it can be also pointed out that the error observed for the reconstruction of the basic flow profiles is smaller than for the secondary one. This is easily understood, since the local velocity or temperature gradients are higher in this latter case, leading to strong local deflections.

Conclusions. – The results presented in this paper show that a good determination of velocity and temperature profiles is possible using an acoustical method based on the time reversal process; the reconstruction of the velocity and temperature profiles, presented in this paper, is performed in the approximation of geometrical acoustics.

A free convection case is numerically investigated and the limitation of such a technique is discussed for application to flows depending on the values of Ma and Ma_T defined in the paper. Works are in progress to experimentally improve this technique; also, perspectives for tomography, both in temperature and velocity, are considered.

$$* * *$$

REFERENCES

[1] GROMOV P. R., EZERSKI A. B . and FABRIKANT A. L., *Sov. Phys. Acoust.*, **28** (1982) 552.
[2] BAUDET C., MICHEL O. and WILLIAMS W. J., *Physica D*, **128** (1999) 1.
[3] SCHMIDT D. W. and TILLMAN P. M., *J. Acoust. Soc. Am.*, **47** (1970) 1310.
[4] MANNEVILLE S., MAUREL A., ROUX P. and FINK M., *Eur. Phys. J. B*, **9** (1999) 545.
[5] MANNEVILLE S., ROBRES J. H., MAUREL A., PETITJEANS P. and FINK M., *Phys. Fluids*, **11** (1999) 3380.
[6] LANDAU L. D. and LIFSHITZ E. M., *Fluid Mechanics*, 2nd edition (MIR, Moscow) 1989, Chapt. 8.
[7] ROUX P. and FINK M., *Europhys. Lett.*, **32** (1995) 25.
[8] GUYON E., HULIN J. P. and PETIT L., *Hydrodynamique Physique* (Intereditions, Editions du CNRS) 1991, p. 446.
[9] ELDER J. W., *J. Fluid Mech.*, **23** (1965) 77.
[10] MANNEVILLE S., MAUREL A., BOTTAUSCI F. and PETITJEANS P., *Vortex Structure and Dynamics*, edited by A. MAUREL and P. PETITJEANS (Springer-Verlag) 1999, p. 231.